Available online at www.sciencedirect.com
ScienceDirect
Physica C 468 (2008) 304–309
PHYSICA C
www.elsevier.com/locate/physc

Boundary effect on superconductivity in long single-crystal superconducting nanowires

Haidong Liu [a], Zuxin Ye [a], Zhiping Luo [b], K.D.D. Rathnayaka [a], Wenhao Wu [a,*]

[a] Department of Physics, Texas A&M University, College Station, Texas 77843, USA
[b] Microscopy and Imaging Center, Texas A&M University, College Station, Texas 77843, USA

Accepted 16 August 2007
Available online 13 November 2007

Abstract

We fabricate single-crystal Pb, Sn, and Zn nanowires, of length 6 or 60 μm and diameter 30–250 nm, using an *in situ* template-based electrochemical method. In this approach, a single nanowire is formed in contact with a pair of bulk film electrodes of Au, Sn, or Pb. We observe that, with superconducting electrodes having a higher critical temperature T_c, superconductivity is induced in Sn and Zn nanowires at the T_c of the electrodes for nanowires as long as 60 μm. With Au electrodes, superconductivity is suppressed completely in 6 μm-long nanowires and partially in 60 μm-long nanowires. Based on transmission electron microscopy studies, the nanowires are single crystalline. Analysis of the temperature dependence of the normalized resistance suggests that the residual-resistance-ratio plays an important role in the observed anomalous long-range proximity effect.

PACS: 74.45.+c; 74.78.Na; 81.07.−b; 82.45.Yz

Keywords: Proximity effect; Nanowires; Porous membrane; Electroplating; Microscopy analysis

1. Introduction

The proximity effect at a superconductor (S) and normal-metal (N) interface has been studied for decades [1–4]. For example, for a bilayer of a low T_{cl} superconductor, such as Al, and a higher T_{ch} superconductor, such as Pb, the critical temperature T_c of the bilayer increases gradually from T_{cl} to T_{ch} with increasing thickness of the Pb film on the Al film. One can also consider similar experiments in which fully normal metals such as Ag can be covered by a superconductor such as Pb. Recently, the proximity effect has been studied in sub-micron to nano-sized interfaces. Of particular interest is the induced superconductivity observed in carbon nanotubes [5–8], semiconductor nanowires [9–11], and graphene sheets [12] of length 0.1–0.5 μm when they are in good contact with superconducting electrodes. It has been shown that this induced superconductivity is often a subtle effect, depending sensitively on the transparency of the interfaces. These observations can be understood in terms of Andreev reflection [13–15] at the S–N interface, which describes the leakage of Cooper pairs from a superconductor into a normal metal. In this process, electrons above the Fermi level in the normal side are converted into holes below the Fermi level and Cooper pairs are formed inside the superconducting side. The electrons and the holes in the normal side form phase-conjugated pairs. Coherence is lost at a certain distance from the interface due to dephasing processes in the normal metal. This length [16] is given by the coherence length in the normal metal L_ϕ and the thermal length L_T which is $2\pi\hbar v_F/k_BT$ in the clean limit and $(\hbar D/k_BT)^{1/2}$ in the dirty limit, where $\hbar$ is Planck's constant, k_B is the Boltzmann constant, v_F is the Fermi velocity, and D is the electron diffusivity.

* Corresponding author. Tel.: +1 979 845 7737; fax: +1 979 845 2590.
E-mail address: wwu@physics.tamu.edu (W. Wu).

0921-4534/$ - see front matter © 2007 Elsevier B.V. All rights reserved.
doi:10.1016/j.physc.2007.08.029

In this paper, we describe an induced superconducting effect in single-crystal Sn and Zn nanowires (NWs) of length up to 60 μm that are in contact with pairs of superconducting electrodes having a higher critical temperature, T_c. The length of our NWs is much longer than the length of the samples used in earlier studies of induced superconductivity in carbon nanotubes [5–8], semiconducting NWs [9–11], and graphene sheets [12]. It is also much longer than the thermal lengths discussed above. For example, the thermal length is about 2 μm at 7 K and 3.8 μm at 3.5 K for Sn in the clean limit. Therefore, the long-range proximity effect we have observed can not be explained by the picture discussed above. Our results provide new evidence that a new mechanism is needed to explain the long-range proximity effect observed in this work as well as in previous experiments [17–19].

2. Sample fabrication

The Pb, Sn, and Zn NWs used for this study were electroplated into porous membranes. Two types of membranes were used: relatively thinner (6 μm) polycarbonate (PC) membranes with random pore sites and thicker (60 μm) anodic aluminum oxide (AAO) membranes with a honeycomb pore arrangement. The PC membranes produced NWs of length 6 μm and diameters 30–200 nm. The AAO membranes produced NWs of length 60 μm and diameters 100–250 nm. The membranes were purchased from Whatman Co. and SPI Supplies Inc. The companies provided the nominal pore diameters for their membranes. These membranes are typically used as filters. As such, the labeled nominal pore diameter reflects the pore diameter in a thin filter layer (~0.4 μm for PC membranes and ~1.5 μm for AAO membranes). For the thicker part of a membrane, the pore diameter is larger. Fig. 1 shows a transmission electron microscopy (TEM) cross-section image of a slice of an AAO membrane prepared by ultramicrotomy. The nominal diameter of the pores was 100 nm. In the TEM image, the thinner filter layer with a smaller pore diameter (~100 nm) can be easily distinguished from the rest of the membrane with a pore diameter 200–250 nm. In this paper, we use the typical NW diameters we observed in microscopy analyses to label the diameters of NWs fabricated using the same batch of membranes.

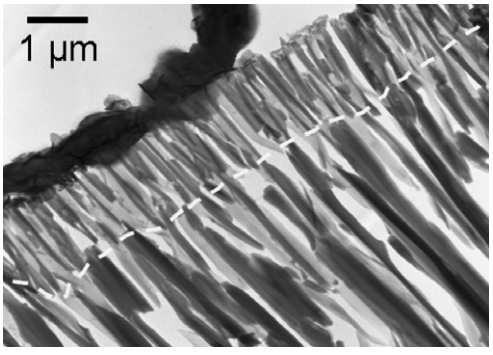

Fig. 1. Cross-section TEM image of a slice of an AAO membrane. The dashed line separates the thinner filter layer having a smaller pore diameter from the rest of the membrane. NWs remaining in their original channels appear as dark contrast. The dark layer at the top is a portion of a Pb back electrode.

We followed a standard electrodeposition procedure, except for an *in situ* contact method which will be discussed below. For depositing Pb NWs, the electrolyte was a 200 ml solution with 16.2 g $Pb(BF_4)_2$ 50 wt% solution in water, 6.72 g HBF_4, and 3.0 g HBO_3. For depositing Sn NWs, the electrolyte was prepared by mixing 16.72 g of a $Sn(BF_4)_2$ solution at 50 wt% with 200 ml of water. For depositing Zn NWs, the electrolyte was prepared by dissolving 4.7 g $ZnCl_2$ into 200 ml water. A Pt anode was used with the reducing potentials relative to an Ag/AgCl reference electrode being 0.4–0.5 V for Pb, 0.4–0.5 V for Sn, and 1.1–1.2 V for Zn.

For carrying out transport measurements on single NWs, we applied an *in situ* method to form electric contacts on single NWs. We first evaporated a thick (~300 nm) Au, Sn, or Pb back electrode on the filter side (see Fig. 1) of a membrane at a tilted angle. It blocked all the pores to form the cathode for electroplating. The anode was placed in the electrochemical cell, facing the other surface of the membrane. Typically, electroplating is initiated at the cathode and the pores are filled to form NWs as positive ions drift into the pores. Various groups [20–29] have used a number of methods to form electric contacts on NWs for transport studies. We applied an *in situ* method [25–27], which allowed us to contact single NWs with a virtually zero contact resistance. In this approach, in addition to the thick back electrode evaporated on the filter side of a membrane, we evaporated a relatively thinner (50–200 nm) front electrode of Au, Sn, or Pb, also at a tilted angle, on the other surface of the membrane. It blocked most of the pores and left only a small number of pores open for electroplating, as illustrated by the left frame in Fig. 2. We used a voltmeter to monitor the potential difference V between the two electrodes. During electroplating, V initially decreased gradually as the open pores were being filled. When the fastest growing NW made a contact with the front electrode, a sudden drop in V was observed.

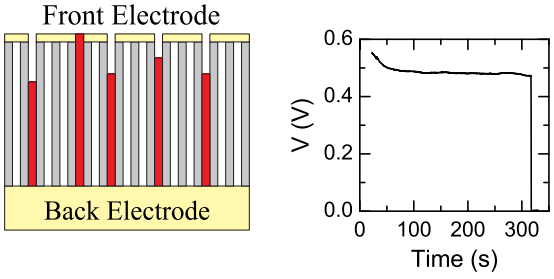

Fig. 2. Left frame illustrates our *in situ* technique for contacting single NWs. Right frame shows the voltage between the front and the back electrode during electroplating.

Electrodeposition was then terminated to obtain a sample having a single NW whose ends were in contact with the back and the front electrodes. Resistance measurements were done with each electrode connected to two measuring wires in a pseudo four-probe configuration to eliminate the resistance of the measuring wires. The results were typically in good agreement [27] with the expected resistance values for single NWs calculated using the dimensions of the NWs and the bulk resistivity of the materials. We believe this *in situ* method produces virtually ideal contacts between a NW and the electrodes with a nearly perfect transparency at the interfaces, probably due to an atomic-scale inter-diffusion layer at the interface. We note that the contact formed between a NW and the back electrode is far more stable then the contact formed between a NW and the front electrode. Thus, we used the filter side of the membrane for the back electrode and the other side with a larger pore diameter for the front electrode.

3. Structure and composition analysis

Our *in situ* contact method can be carried out only if the NW material electroplated into the pores has a higher reactivity than that of the electrodes. Otherwise, the front electrode became reactive and would peel off during electroplating. When the reactivity of the NW material is higher than that of the electrode material, it is impossible for electrode materials to be mixed into the NWs. To confirm this and to investigate the structure of the NWs, we have carried out extensive transmission electron microscopy (TEM) and scanning electron microscopy (SEM) analyses.

For TEM investigation of extracted NWs, the back and the front electrodes were first gently polished off a membrane, which was then dissolved (in 1 M NaOH solution for AAO membranes or in dichloromethane for PC membranes). NWs were extracted using a centrifuge. Free standing NWs in ethanol or water can be placed on a Cu grid for TEM and SEM studies. The top frame in Fig. 3 is a typical TEM image of a Zn NW grown with Pb electrodes. Selected-area electron diffraction (SAED) patterns, shown in the inset to the top frame and taken on different spots along the NW, revealed the same geometry without rotation, indicating that the NWs were single crystalline. Plane indexes and growth direction are marked on the SAED pattern, from which the Zn NWs were found to have a hexagonal structure, as that of the superconducting bulk phase. Sn and Pb NWs grown on various back electrodes were also found to be single crystalline. The lower frame in Fig. 3 shows an energy dispersion spectroscopy (EDS) taken on the Zn NW in the top frame. Besides C and Cu, associated with the TEM sample grid, and O, associated with an oxide layer on the NW, peaks associated with Pb near 10.5 keV and 12.7 keV were clearly absent. Therefore, the possibility of mixing of Pb from the electrode into the Zn NW can be excluded. Similar EDS studies performed on many NWs grown with various electrodes have not found any sign of mixing of materials from the electrodes into the NWs. Imaging of NWs was also carried out for NWs remaining in their original pore channel, in thin slices of membranes produced by ultramicrotomy, as shown in Fig. 1.

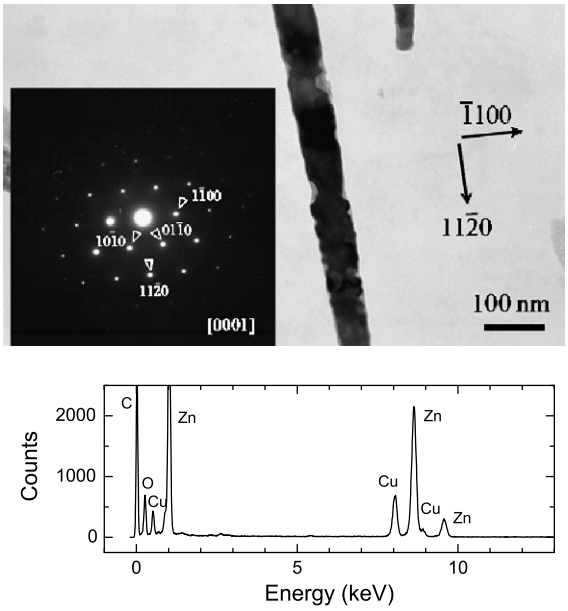

Fig. 3. Top: TEM image of a Zn NW with selected area electron diffraction. Bottom: EDS taken from the Zn NW. The C and Cu peaks were from the TEM sample grid. The O peak was likely from an oxide layer on the NW. Peaks for Pb at 10.5 keV and 12.7 keV are absent.

4. Long-range proximity effect

We measured the resistance R of single NWs of Pb, Sn, and Zn down to 1.8 K using a Quantum Design physical properties measurement system (PPMS) with a 9-T superconducting magnet. We note that the critical temperatures for bulk Pb, Sn, and Zn are, respectively, $T_c(\mathrm{Pb}) = 7.2$ K, $T_c(\mathrm{Sn}) = 3.7$ K, and $T_c(\mathrm{Zn}) = 0.88$ K. In Fig. 4, we plot R vs. T for a number of Sn (left frames) and Zn (right frames) NWs of various diameters that were in contact with pairs of electrodes of either Au, Sn, or Pb. These NWs were 6 μm in length, fabricated using PC membranes. We observe in Fig. 4a that Sn NWs did not show any signature of superconductivity down to 1.8 K when they were in contact with Au electrodes. While T_c(Zn) was outside the accessible temperature range of the PPMS, similar measurements with Pb NWs in contact with Au electrode also observed complete suppression of superconductivity down to 1.8 K. In Fig. 4b and e, we observe that both Sn and Zn NWs were superconducting at T_c(Sn) when they were in contact with Sn electrodes. In Fig. 4c and f, we observe that both Sn and Zn NWs were superconducting at T_c(Pb) when they were in contact with Pb electrodes. Thus, we conclude that superconductivity is completely suppressed in 6 μm-long Sn NWs by Au electrodes. When in contact

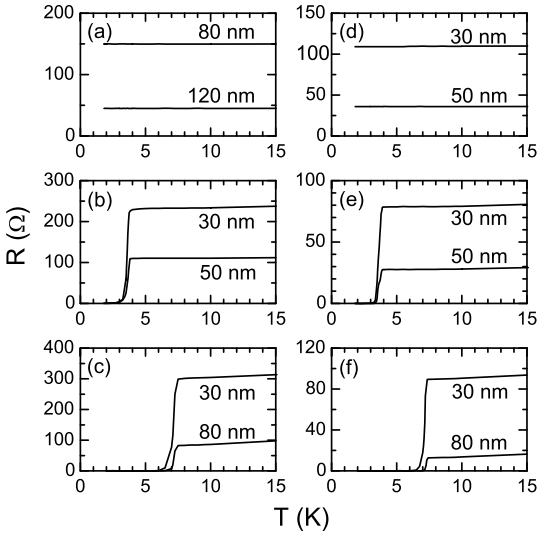

Fig. 4. R vs T for Sn (left frames) and Zn (right frames) NWs in contact with pairs of Au (top), Sn (middle), or Pb (lower) electrodes. The diameters of the NWs are indicated.

with electrodes having a higher T_c, superconductivity is induced in these NWs at the T_c of the electrodes.

In Fig. 5 we plot R vs T for 60 μm-long Sn and Zn NWs in contact with Pb electrodes. The induced superconductivity in these long NWs at T_c(Pb) was as robust as the induced superconductivity observed in 6 μm-long NWs. In Fig. 6, we plot R vs T measured on 60 μm-long Pb NWs. The Pb NWs were superconducting at T_c(Pb) with a zero residual resistance when in contact with Pb electrodes. When in contact with Au electrodes, there was still a superconducting transition at T_c(Pb), but there was a significant residual resistance well below T_c(Pb). Therefore, the suppression of superconductivity by Au electrodes in these long nanowires was only partial. This was also observed in 60 μm-long Sn NWs.

We also applied a magnetic field to suppress superconductivity in both the NWs and the electrodes. This provided another means to investigate how superconductivity in the NWs depended on the superconductivity in the electrodes. We measured simultaneously the resistive transitions of NWs and the electrodes. In Fig. 7, we plot R vs. T for a Sn NW at various magnetic fields applied transverse to

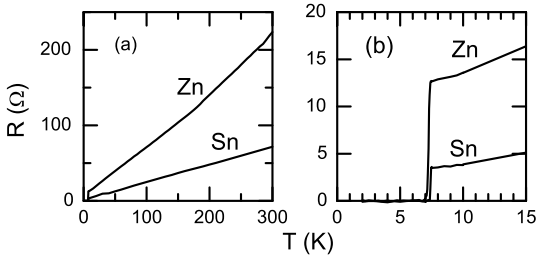

Fig. 5. The left frame shows R vs T up to 300 K for one Zn and one Sn NWs in contact with Pb electrodes. The right frame shows transitions at the critical temperature of Pb for the Zn and Sn NWs in contact with Pb electrodes.

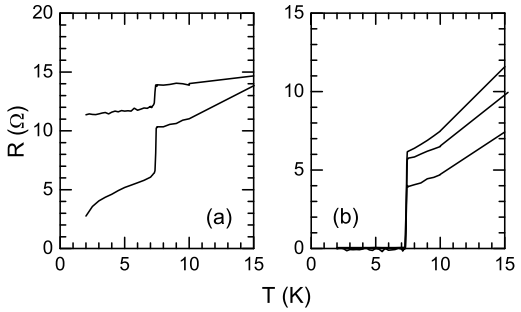

Fig. 6. (a): R vs T for 60 μm-long Pb NWs in contact with Au electrodes, showing a partial transition with a significant residual resistance at low T. (b): With Pb electrodes, Pb NWs show transition without a residual resistance.

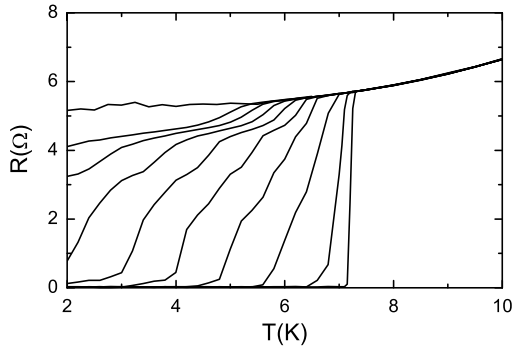

Fig. 7. R vs T for a 60 μm-long Sn NW in contact with Pb electrodes, at transverse fields of 0, 0.2, 0.4, 0.6, 0.8, 1.0, 1.2, 1.4, 1.6, and 3.0 kOe for curves from left to right showing the field suppression of superconductivity in the Sn NW.

the NW, showing a shift of the transition toward lower temperatures with increasing field. This Sn NW was 60 μm in length and 200 nm in diameter, and in contact with a pair of Pb electrodes. In Fig. 8b, we plot resistance vs field at three temperatures measured on one Pb electrode in contact with the Sn NW, with the field aligned in parallel with the plane of the Pb electrode (transversed to the Sn NW). We obtained the critical temperatures and the critical fields at the mid point of the resistive transitions. The dependence of the critical temperatures on magnetic field is shown by Fig. 8a for data obtained from curves in Figs. 7 and 8b. Fig. 8a shows that the transition of the Sn NW followed

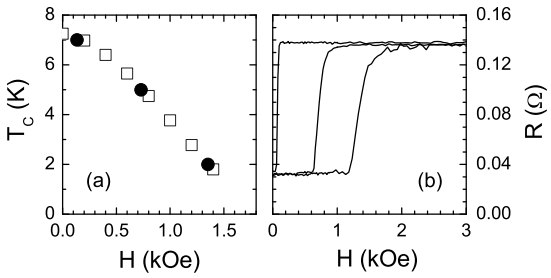

Fig. 8. (a): Open squares show the critical temperature vs transverse field for the Sn NW in Fig. 7. Solid circles show the critical field vs temperature for one Pb electrode in contact with the same Sn NW, obtained from curves in (b). (b): Resistive transitions for this Pb electrode measured at 7 K, 5 K, and 2 K, for curves from left to right.

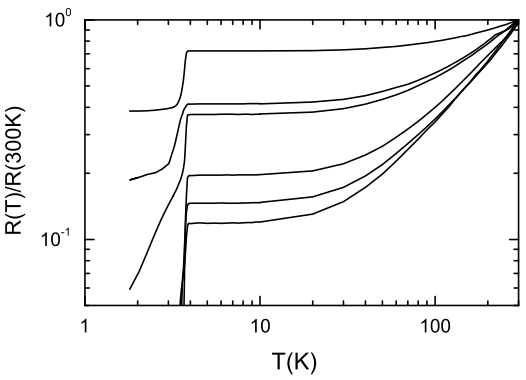

Fig. 9. Normalized R vs T for a number of Zn NWs in contact with Sn electrodes, showing a sharp drop of residual resistance below T_c with increasing RRR values.

precisely the transition of the Pb electrode, providing direct evidence for a long-range proximity effect in the NWs.

The long-range proximity effect described above have been observed consistently in virtually all the samples (~120) of various NW/electrode combinations we have measured so far. These NWs were single crystalline with residual-resistance-ratio (RRR) values in the range of 1.4 to 50. We are not sure exactly how to control growth to produce NWs of desirable RRR values. In Fig. 9, we plot the normalized resistance versus temperature curves for Zn NWs grown in PC membranes with Sn electrodes. We note that the inverse of the normalized resistance value in the flat region right above the critical temperature gives the value of RRR. This figure shows clearly that the critical temperature of the Zn NWs is shifted to T_c(Sn) with Sn electrode and this observation did not seem to depend on the value of RRR. However, the residual resistance below the critical temperature was sensitively dependent upon the value of RRR. The induced superconductivity was partial for NWs having small RRR values of less than 2.5. For RRR larger than 2.5, the residual resistance dropped to zero quickly. We estimate the upper limit of the coherence length using the thermal length in the clean limit for NWs with large values of RRR, $L_T = 2\pi\hbar v_F/k_B T$. It is about 1.9 μm at 7.2 K and 3.7 μm at 3.7 K for Zn. This is comparable to one-half of the length of 6 μm-long NWs. The leakage of normal currents from both ends into a superconducting NW over this length could explain the suppression of superconductivity completely in 6 μm-long NWs and partially in 60 μm-long by Au electrodes. However, it is much too short to account for the induced superconductivity in 60 μm-long NWs. Therefore, the observed long-range proximity effect is not understood based on existing theories. Fig. 9 suggests that the value of RRR plays an important role in this anomalous long-range proximity effect.

5. Conclusions

Using an *in situ* template-based electrochemical methode, we fabricated single nanowires of Pb, Sn, and Zn, of length 6 or 60 μm and diameter 30–250 nm, which were in contact with a pair of bulk film electrodes of Au, Sn, or Pb. We observed that, with superconducting electrodes having a higher critical temperature T_c, superconductivity was induced in Sn and Zn NWs at the T_c of the electrodes for NWs as long as 60 μm. With Au electrodes, superconductivity was suppressed completely in 6 μm-long NWs and partially in 60 μm-long NWs. TEM studies demonstrated that the NWs were single crystalline. These studies also ruled out the possibility of mixing of electrode materials into the NWs. Analysis of the temperature dependence of the normalized resistance suggests that the value of RRR plays an important role in the observed anomalous long-range proximity effect.

Acknowledgements

We thank V. Pokrovsky, D. G. Naugle, and J. Ross for useful discussions. This work was supported by NSF under Grant Nos. DMR-0551813 and DMR-0606529. The PPMS was funded by NSF under Grant No. DMR-0315476.

References

[1] P.G. de Gennes, Rev. Mod. Phys. 36 (1964) 225.
[2] P.G. de Gennes, Superconductivity of Metals and Alloys, Benjamin, New York, 1966.
[3] G. Deutscher, P.G. de Gennes, in: R.D. Parks (Ed.), Superconductivity, vol. 2, Marcel Dekker, New York, 1969, p. 1005.
[4] S.T. Ruggiero, M.R. Beasley, in: L.I. Chang, B.C. Giessen (Eds.), Synthetic Modulated Structures, Academic, New York, 1985, p. 313.3.
[5] A.Yu. Kasumov, R. Deblock, M. Kociak, B. Reulet, H. Bouchiat, I.I. Khodos, Yu.B. Gorbatov, V.T. Volkov, C. Journet, M. Burghard, Science 284 (1999) 1508.
[6] A.F. Morpurgo, J. Kong, C.M. Marcus, H. Dai, Science 286 (1999) 263.
[7] M.R. Buitelaar, T. Nussbaumer, C. Schönenberger, Phys. Rev. Lett. 89 (2002) 256801.
[8] P. Jarillo-Herrero1, J.A. van Dam, L.P. Kouwenhoven, Nature 439 (2006) 953.
[9] Y.J. Doh, J.A. van Dam, A.L. Roest, E.P.A.M. Bakkers, L.P. Kouwenhoven, S. De Franceschi, Science 309 (2005) 272.
[10] J.A. van Dam, Y.V. Nazarov, E.P.A.M. Bakkers, S. De Franceschi, L.P. Kouwenhoven, Nature 442 (2006) 667.
[11] J. Xiang, A. Vidan, M. Tinkham, R.M. Westervelt, C.M. Lieber, Nature Nanotechnol. 1 (2006) 208.
[12] H.B. Heersche, P. Jarillo-Herrero, J.B. Oostinga, L.M.K. Vandersypen, A.F. Morpurgo, Nature 446 (2007) 56.
[13] A.F. Andreev, Zh. Eksp. Theor. Fiz. 46 (1964) 1823, Sov. Phys. JETP 19 (1964) 1228.
[14] G.E. Blonder, M. Tinkham, T.M. Klapwijk, Phys. Rev. B 25 (1982) 4515.
[15] T.M. Klapwijk, J. Supercond. 17 (2004) 593.
[16] F. Zhou, B. Spivak, A. Zyuzin, Phys. Rev. B 52 (1995) 4467.
[17] Y.K. Kwong, K. Lin, M.S. Isaacson, J.M. Parpia, Phys. Rev. Lett. 65 (1990) 2905.
[18] Y.K. Kwong, K. Lin, M. Park, M.S. Isaacson, J.M. Parpia, Phys. Rev. B 45 (1992) 9850.
[19] H. Courtois, Ph. Gandit, B. Pannetier, Phys. Rev. B 52 (1995) 1162.
[20] T.M. Whitney, P.C. Searson, J.S. Jiang, C.L. Chien, Science 261 (1993) 1316.
[21] L. Piraux et al., Appl. Phys. Lett. 65 (1994) 2484.

[22] A. Blondel, J.P. Meier, B. Doudin, J.-Ph. Ansermet, Appl. Phys. Lett. 65 (1994) 3019.
[23] K. Liu, C.L. Chien, P.C. Searson, K. Yu-Zhang, Appl. Phys. Lett. 73 (1998) 1436.
[24] Z. Zhang, X. Sun, M.S. Dresselhaus, J.Y. Ying, J. Heremans, Phys. Rev. B 61 (2000) 4850.
[25] Y. Jaccard, Ph. Guittienne, D. Kelly, J.-E. Wegrowe, J.-Ph. Ansermet, Phys. Rev. B 62 (2000) 1141.
[26] F. Elhoussine, S. Mátéfi-Tempfli, A. Encinas, L. Piraux, Appl. Phys. Lett. 81 (2002) 1681.
[27] W. Wu, J.B. DiMaria, H.G. Yoo, S. Pan, L.J. Rothberg, Y. Zhang, Appl. Phys. Lett. 84 (2004) 966.
[28] M. Tian, N. Kumar, S. Xu, J. Wang, J.S. Kurtz, M.H.W. Chan, Phys. Rev. Lett. 95 (2005) 076802.
[29] M. Tian, N. Kumar, J. Wang, S. Xu, M.H.W. Chan, Phys. Rev. B 74 (2006) 014515.